A Dynamic Model for Low-Pressure, Hollow-Fiber Ultrafiltration

R. P. MA, C. H. GOODING, and W. K. ALEXANDER

Department of Chemical Engineering
Clemson University
Clemson, SC 29631

One of the common ultrafilter designs is the hollow-fiber configuration in which the membrane is formed on the inside of tiny polymer cylinders that are then bundled and potted into a tube-and-shell arrangement. The tubeside feed-concentrate flow is invariably laminar due to the small diameter. Axial pressure drop and concentration polarization can have a significant effect on the permeate flux achieved in these units, particularly when the feed pressure is relatively low.

Several theoretical models have been published to predict and correlate mass transfer phenomena in tubular membrane geometries, most often with reference to high-pressure reverse osmosis units. The usual approach is to obtain a perturbation solution of the Navier-Stokes equations and then to use the resulting velocity profiles to effect an approximate analytical or numerical solution of the solute continuity equation. For example, Gill et al. (1971) developed a solution for the case in which, among other assumptions, axial pressure drop and osmotic pressure are negligible. Permeate flux is thus constant with respect to axial position in the separator. They also presented results that took osmotic pressure into account but still neglected axial pressure drop. The assumption of spatially uniform permeate flux was invoked by Doshi and Gill (1975) in a paper on unsteady-state effects and by Singh and Laurence (1979) in a study of the effect of slip velocity at the membrane. Hieber (1974) and Chang and Guin (1978) accounted for the axial variation in osmotic pressure in their investigations of natural convection but neglected the axial drop in hydraulic pressure.

The primary objective of this study was to develop and test a numerical solution of the pertinent equations that would account for axial variation in both the hydraulic pressure and the osmotic pressure. The focus, as noted above, is on low-pressure ultrafiltration systems in which both axial pressure drop and concentration polarization have significant effects on permeate flux.

MATHEMATICAL MODEL

The model was developed to simulate forced-convection ultrafiltration in a horizontal, tubular or hollow-fiber membrane system. The feed-concentrate stream on the inside of the membrane tubes is laminar, and mass density, viscosity, and solute diffusivity are assumed to be constant. In dimensionless form and cylindrical coordinates, the equation of continuity for the solute becomes

$$\frac{\partial C}{\partial \tau} + U\frac{\partial C}{\partial Z} + \left(V - \frac{1}{PeR}\right)\frac{\partial C}{\partial R} = \frac{1}{Pe}\frac{\partial^2 C}{\partial R^2}. \tag{1}$$

Axial diffusion and angular effects (e.g., due to natural convection) are ignored. The initial and boundary conditions are

$$C(0,R,Z) = 1, \tag{2}$$

$$C(\tau,R,0) = 1, \tag{3}$$

$$\left(\frac{\partial C}{\partial R}\right)_{R=0} = 0, \tag{4}$$

$$\left(\frac{\partial C}{\partial R}\right)_{R=1} = VCPe. \tag{5}$$

The transient term is left in Eq. 1 to yield potentially useful information on the dynamics of the process since an iterative technique is required to obtain the steady-state solution anyway. Equations 2 and 3 denote constancy of the feed solute concentration, Eq. 4 assumes radial symmetry, and Eq. 5 is a solute mass balance written at the membrane surface, assuming perfect solute rejection.

Yuan and Finkelstein (1956) used a perturbation technique to solve the Navier-Stokes equations and obtain steady-state velocity profiles for laminar flow through a porous tube. For the small values of permeation velocity and tube radius that are appropriate to this work, their results reduce to the dimensionless equations

$$U = 2(1 - 2V_m Z)(1 - R^2), \tag{6}$$

$$V = V_m(2R - R^3). \tag{7}$$

Strictly, these velocity profiles apply only to the case of constant permeation velocity, but this restriction is circumvented by the numerical solution technique explained in the next section.

The membrane permeation velocity is evaluated from the expression

$$v_m = K(P_m - P_s - \pi_m). \tag{8}$$

The membrane permeability constant is determined from flux vs. pressure drop tests with pure solvent or, in our case, with a saline solution. No allowance is made in the model for a decrease in permeability due to gel formation, which can occur at high surface solute concentrations. The permeate back-pressure is assumed to be constant, but the tubeside pressure depends on axial position. With a constant, low permeation velocity and small tube radius, Yuan and Finkelstein's work predicts the steady-state, axial pressure distribution to be

Correspondence concerning this work should be addressed to C. H. Gooding. R. P. Ma is now a doctoral candidate at North Carolina State University, Raleigh, NC.

$$P_o - P_m(z) = \frac{8\mu\bar{u}_o z}{r_m^2}\left[1 - \frac{v_m z}{\bar{u}_o r_m}\right]. \quad (9)$$

Our experimental measurements of overall axial pressure drop were consistently 50% higher than the values predicted from Eq. 9. Conceivable sources of this discrepancy include increased viscosity due to concentration polarization in the high shear region near the membrane, and inaccuracy in the nominal fiber radius (a 10% error in radius would account for the entire discrepancy since $[P_o - P_m(z)] \propto r_m^{-4}$ at low permeation velocities). Since we were unable to resolve this discrepancy, we adopted a simpler expression based on the observed, overall pressure drop,

$$P_o - P_m(z) = \Delta P_{ax}\frac{z}{L}. \quad (10)$$

The osmotic pressure in Eq. 8 is a function of solute concentration at the membrane surface. Perfect solute rejection is assumed. For the bovine albumin used in this work the osmotic pressure-composition relationship was determined from the work of Scatchard et al. (1946). At 37°C and a pH of 6.7 the empirical relationship reduces to the polynomial form

$$\pi\ (\text{mm Hg}) = 0.279w + 1.83 \times 10^{-3} w^2 + 3.66 \times 10^{-6} w^3. \quad (11)$$

Solute diffusivity is an important parameter of the Peclet number in Eq. 1. For albumin in saline at 25°C, Keller et al. (1971) reported a diffusivity of 7×10^{-7} cm^2/s at low concentration, but only 2×10^{-7} cm^2/s at 20% albumin. Phillies et al. (1976) reported values in the range of 5 to 8×10^{-7} cm^2/s at 25°C with various buffers and pH levels, but found virtually no protein concentration dependence. For our work at 37°C we used a constant value of 9×10^{-7} cm^2/s, which is consistent with 7×10^{-7} cm^2/s at 25°C ($D \propto T/\mu$) and negligible concentration dependence.

NUMERICAL SOLUTION OF THE MODEL

Drawing from several methods illustrated in von Rosenberg (1969) we developed a finite-difference solution technique for the model. To represent the two spatial dimensions and the time step, a three-dimensional grid was established. Equation 1 was then written at the center of each grid space using modified centered-difference analogs for the time and axial derivatives, and modified Crank-Nicolson analogs for the radial derivatives. Preliminary solutions established the presence of steep concentration gradients in the axial direction near the tube inlet and in the radial direction near the membrane surface. To provide reasonable accuracy in the finite-difference approximations and still conserve computing time, a split grid arrangement was used with finer axial grid spacing near the tube inlet and finer radial spacing near the membrane. Special finite-difference analogs were written at the interfaces of unequal grid size.

The solution sequence starts at the first axial grid increment and the first unknown time step. Each axial increment is treated as a separate membrane tube with constant tubeside pressure and permeation velocity. The solute concentration at the membrane surface is estimated and the permeation velocity is calculated from Eq. 8 using the osmotic pressure from Eq. 11. The velocity profiles are then calculated from Eqs. 6 and 7. The finite difference analog to Eq. 1 is written for each radial grid position, using Eqs. 2 through 5 where appropriate, and the resulting equations are put into tridiagonal matrix form and solved via the Thomas algorithm. The calculated concentration at the membrane surface is compared to the estimated value, and the procedure is iterated to convergence using the regula-falsi method. Convergence to 0.5% is usually obtained in three or four iterations.

When the radial profile is established at one axial increment, the program proceeds to the next axial increment. The new tubeside pressure is calculated from Eq. 10. After the last axial increment is calculated, the converged permeation velocities are multiplied by the incremental surface areas and summed to give the total permeation rate. The solution then progresses to the next time step and continues until a steady-state ultrafiltration rate is predicted.

The numerical solution of the model equations was obtained via a WATFIV program run on an IBM 370/3033 computer. Convergence studies were run to determine the number and size of axial and radial increments required to obtain a unique solution. The final grid arrangement consisted of 40 small radial increments near the membrane surface and 32 increments over the remaining radius with the interface 20% of the radial distance from the membrane. Axially we used 20 small increments over the first 10% of the length and 10 large increments over the remaining 90%. A realtime step equal to 1% of the nominal residence time ($L/\bar{u}_o$) was sufficient to insure convergence. For individuals runs, CPU time ranged from 1 to 4 min.

EXPERIMENTS

The steady-state predictions of the mathematical model were compared to experimental data on the ultrafiltration of protein solutions. An Amicon model H1P10 hollow-fiber cartridge (Amicon Corp., Danvers, MA) was used in the experiments. Each of the 1,000 fibers in the cartridge was a 200 μm I.D., anisotropic, noncellulosic membrane rated for a 10,000 molecular weight cutoff. The measured active length of the fibers between the epoxy headers was 17 ± 0.2 cm.

TABLE 1. EXPERIMENTAL RESULTS AND MODEL PREDICTIONS

Run No.	ΔP_{ax} mm Hg	ΔP_{re} mm Hg	Conc. Rate cm^3/s	Perm. Rate cm^3/s	Pred. Perm. Rate cm^3/s
1	46	93	0.84	0.40	0.42
2	40	92	0.61	0.38	0.36
3	37	100	0.45	0.39	0.34
4	32	146	0.37	0.46	0.43
5	43	180	0.62	0.58	0.58
6	53	191	0.89	0.58	0.57
7	51	155	0.81	0.54	0.51
8	50	138	0.83	0.52	0.49
9	51	95	0.94	0.43	0.43
10	37	185	0.35	0.50	0.50

SI conversion: kPa = mm Hg × 0.133.

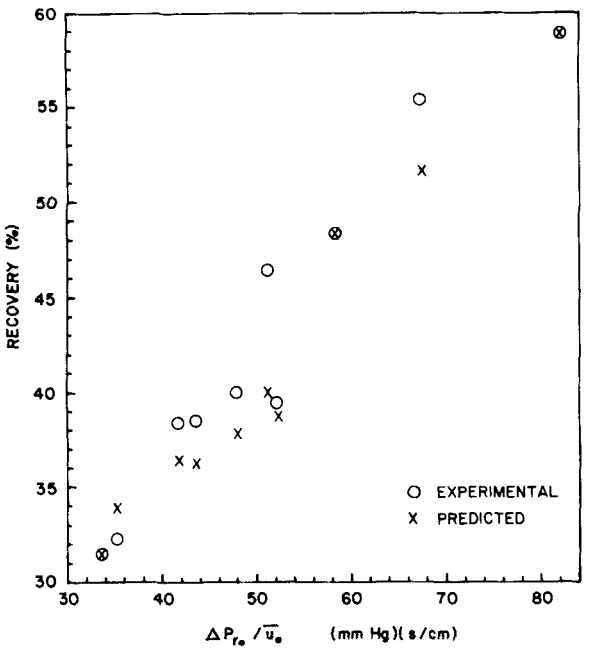

Figure 1. Graphical comparison of experimental and predicted results.

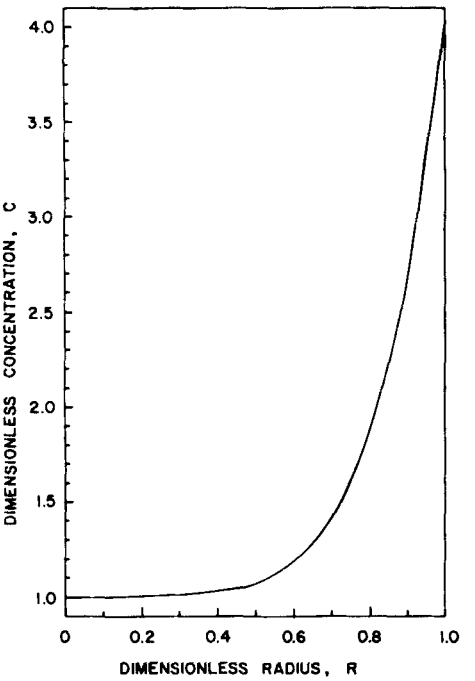

Figure 3. Calculated steady-state radial solute profile at a hollow-fiber exit (run 7).

All membrane permeability tests and ultrafiltration experiments were conducted at 37°C. The membrane permeability was determined from flux vs. pressure drop measurements with distilled water and with saline solution and in both static and dynamic tests. In the dynamic tests the flux was correlated with average transmembrane pressure drop, $\Delta P_{re} + (\Delta P_{ax})/2$. In all four types of tests the permeability constant was determined to be 3.8×10^{-6} cm/s mm Hg. For filtration runs the feed was 2 mass % bovine albumin (*U.S. Biochemical Corp., Cleveland, OH*) in a 0.88% saline solution at a pH of 6.7. The feed for each run passed through a 0.8 μm prefilter prior to entering the cartridge. During each run a sample of feed entering the cartridge was collected for a precise, pycnometric determination of protein concentration. Timed volumetric collections were made of concentrate and permeate until steady-state rates were achieved. The permeate was tested via nitric acid addition to verify the absence of protein.

RESULTS AND DISCUSSION

Pertinent steady-state experimental results and model predictions are summarized in Table 1. The model input included inlet velocity calculated from the measured concentrate and permeate flow rates, transmembrane pressure drop at the cartridge exit, and axial pressure drop. The absolute deviation between the measured and predicted permeation rates averaged 4.3% of the measured rate with six of the ten predictions being on the low side. Regression analyses were run to test for the potential significance of neglected effects, e.g., natural convection and concentration dependence of diffusivity. With percent deviation as the dependent variable, individual linear regressions were run against recovery (permeate rate/feed rate), transmembrane pressure drop, feed velocity, nominal feed residence time, predicted maximum surface concentration, and predicted permeation rate. None of the correlation coefficients exceeded 0.2.

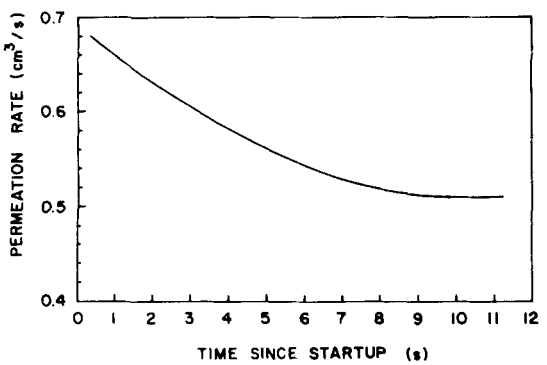

Figure 2. Calculated approach of run 7 to a steady-state permeation rate.

Figure 1 is a convenient graphical comparison of the experimental results and the model predictions. A nearly linear plot such as Figure 1 might be used to predict ultrafilter performance from a few data points without rigorous modeling of the process, but the result could be misleading because the plot does not extrapolate to a zero intercept as one might expect; i.e., it is not linear in the lower range of recoveries. Protein ultrafiltration data reported by Wendt et al. (1981) indicated that permeation rate in a hollow-fiber module is virtually independent of axial velocity. The average flux in their module was about one-tenth of the flux in our Amicon units. Our Figure 1 shows that the dependence on axial velocity is weak but not completely absent. The ordinate is directly proportional to average flux over inlet axial velocity, $\bar{u}_o$. Multiplying the abscissa and ordinate by $\bar{u}_o$ would eliminate $\bar{u}_o$ as a parameter only if the intercept were zero. We found that a plot of permeation rate (measured or predicted) vs. transmembrane pressure drop alone yielded a poorer correlation than Figure 1.

The model can yield considerable information that is of practical interest. Using run 7 as a typical example, Figure 2 shows that the ultrafilter approaches steady state rather quickly after permeation begins. In this work nominal residence times based on inlet velocity ranged from 3.6 to 6.4 sec. Figure 3 illustrates concentration polarization with a plot of the steady-state dimensionless radial con-

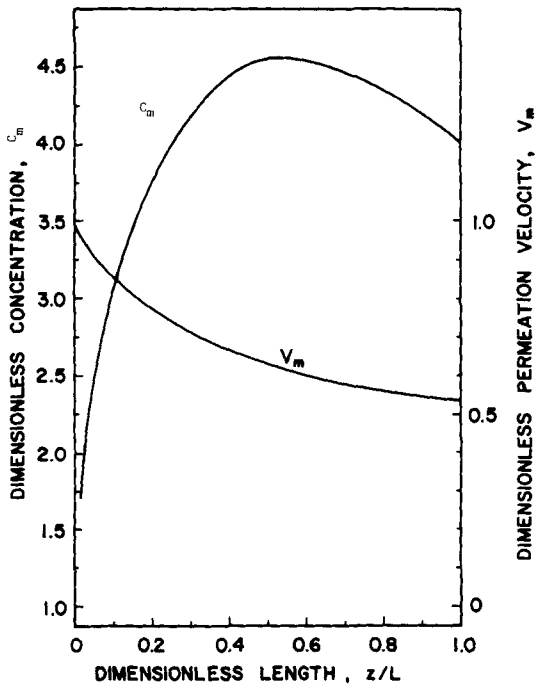

Figure 4. Calculated steady-state axial profiles of surface solute concentration and permeation velocity (run 7).

centration profile at the exit of a hollow fiber. For this run the bulk average solute concentration leaving the ultrafilter was 1.67 times the feed concentration (recovery = 40%), but the surface concentration was more than twice as large.

Figure 4 shows steady-state dimensionless axial profiles of permeation velocity and solute concentration at the membrane surface. Based on Eq. 8 alone, one might expect C_m to rise monotonically until $\pi_m = P_m - P_s$ and V_m goes to zero. But surface concentration and permeation velocity are also related through Eq. 5, which says that concentration polarization is sustained only by convection of solute to the membrane with solvent. In other words, C_m may peak as shown in Figure 4 and then drop off as V_m continues to decline toward the fiber exit. The relationship is complicated further when V_m is influenced significantly by axial pressure drop. In other simulations with the model we observed that axial pressure drop can dissipate the driving force for solvent flux to the extent that flux reversal (osmosis) will occur near the exit end of the tube. This extreme behavior occurred at low values of $\Delta P_{ro}/\bar{u}_o$, on the order of 10 mm Hg s/cm in our simulations.

SUMMARY AND CONCLUSIONS

A low-pressure, hollow-fiber ultrafiltration system has been modeled successfully by numerically solving the solute continuity equation. The model requires prior knowledge of the membrane permeability constant for pure solvent, the solute diffusivity, and the solute concentration-osmotic pressure relationship. Input specifications are inlet transmembrane pressure drop, feed rate, and overall axial pressure drop. With further work, we hope to eliminate the need to specify axial pressure drop.

The finite-difference approach allows solution of the model for the case in which both axial pressure drop and osmotic pressure have a significant effect on membrane flux. The model can be used to predict flux or to investigate other important considerations, such as the possibility of solute precipitation or gel formation due to concentration polarization, or the reversal of flux in high-throughput, low-pressure systems. The model may also prove useful in establishing the applicable ranges of simpler analytical models of ultrafiltration.

NOTATION

C = dimensionless solute concentration, c/c_o
c = mass concentration of solute
D = diffusivity of solute in solvent
K = membrane permeability constant
L = length of hollow fibers
P = fluid pressure
ΔP = pressure drop
Pe = initial Peclet number, $v_{mi}r_m/D$
R = dimensionless radial coordinate, r/r_m
r = radial coordinate
T = absolute temperature
t = time
U = dimensionless axial velocity, $u/\bar{u}_o$
u = axial velocity
V = dimensionless radial velocity, v/v_{mi}
v = radial velocity
w = mass ratio, g protein/1,000 g water
Z = dimensionless axial coordinate, $zv_{mi}/\bar{u}_o r_m$
z = axial coordinate

Greek Letters

μ = viscosity
π = osmotic pressure
τ = dimensionless time, tv_{mi}/r_m

Subscripts

ax = overall axial parameter
e = exit value
i = initial value
m = tubeside value at membrane surface
o = inlet (feed) value
r = radial or transmembrane parameter
s = shellside value
z = axial parameter

Superscript

$\bar{}$ = spatially averaged value

LITERATURE CITED

Chang, C. Y., and J. A. Guin, "Combined Forced and Free Convection in a Reverse Osmosis System," *AIChE J.*, **24**, 1,046 (1978).
Doshi, M. R., and W. N. Gill, "Unsteady Reverse Osmosis or Ultrafiltration in a Tube," *Chem. Eng. Sci.*, **30**, 1,467 (1975).
Gill, W. N., L. J. Derzansky, and M. R. Doshi, "Convective Diffusion in Laminar and Turbulent Hyperfiltration (Reverse Osmosis) Systems," *Surface and Colloid Science*, E. Matijevic, Ed., Wiley, New York, **4**, 261 (1971).
Hieber, C. A., "A Buoyancy-Dominated Desalination Unit," *Desalination*, **15**, 59 (1974).
Keller, K. H., E. R. Canales, and S. I. Yum, "Tracer and Mutual Diffusion Coefficients of Proteins," *J. Phys. Chem.*, **75**, 379 (1971).
Phillies, G. D. J., G. B. Benedek, and N. A. Mazar, "Diffusion in Protein Solutions at High Concentrations: A Study by Quasielastic Light Scattering Spectroscopy," *J. Chem. Phys.*, **65**, 1,883 (1976).

Scatchard, G., et al., "Preparation and Properties of Serum and Plasma Proteins. VII: Osmotic Equilibria in Concentrated Solutions of Serum Albumin," *J. Am. Chem. Soc.*, **68**, 2,610 (1946).

Singh, R., and R. L. Laurence, "Influence of Slip Velocity at a Membrane Surface on Ultrafiltration Performance. II: Tube Flow System," *Int. J. Heat Mass Transfer*, **22**, 731 (1979).

von Rosenburg, D. U., *Methods for the Numerical Solution of Partial Differential Equations*, Elsevier, New York, 22–25, 75–77, 95–99, 113 (1969).

Wendt, R. P., et al., "Hollow Fiber Ultrafiltration of Calf Serum and Albumin in the Pregel Uniform-Wall-Flux Region," *Chem. Eng. Commun.*, **8**, 251 (1981).

Yuan, S. W., and A. B. Finkelstein, "Laminar Pipe Flow with Injection and Suction Through a Porous Wall," *Trans. ASME*, **78**, 719 (1956).

Manuscript received July 6, 1984; revision received Oct. 17 and accepted Oct. 29, 1984.